11th AIAA Aviation Technology, Integration, and Operations (ATIO) Conference, including the AIA
20 - 22 September 2011, Virginia Beach, VA

AIAA 2011-7068

Wind Tunnel Study of a Large Aerostat

Stephen C. Chan[1] and John D. Hunt[2]
TCOM, L.P., Columbia, MD 21046

To further the development of larger and more capable aerostats at TCOM, an update to the aerodynamic database was needed. This lead to comprehensive wind tunnel testing conducted in the Glenn L. Martin (GLM) Wind Tunnel at the University of Maryland in 2010. Various studies included comparison to the historical database, wind speed effects, and configuration effects. The configuration effects included a lower fin anhedral angle study and obtaining the effects of each of the individual configuration modules in order to properly isolate each effect. The modules consist of the hull, windscreen, and fins. Test data obtained included force and moment coefficients, pressure distributions, and flow visualizations. This verified dataset will continue to improve and validate tools and analyses, including CFD and inputs to the FEM.

Nomenclature

α	=	angle of attack, Alpha in degrees
β	=	angle of sideslip, Beta in degrees
ψ	=	angle of yaw, Psi in degrees = -β
C_D	=	drag force coefficient
C_L	=	lift force coefficient
C_m	=	pitching moment coefficient
C_n	=	yawing moment coefficient
C_p	=	pressure coefficient
C_S	=	side force coefficient
CFD	=	computational fluid dynamics
c	=	reference length, length of the hull
H	=	hull
WS	=	windscreen
F	=	fins with lower fins at the baseline anhedral angle
F@Low	=	fins with lower fins at the lower anhedral angle
FEM	=	finite element model
GLM	=	Glenn L. Martin (wind tunnel)
S	=	hull reference area = $V^{2/3}$
UT	=	University of Toronto Institute for Aerospace Studies (historically used wind tunnel)
V	=	hull volume
V_∞	=	freestream velocity

I. Introduction

RECENT technological innovations have allowed for economically feasible designs of larger lighter than air vehicles. Larger vehicles, which are defined as in excess of 2,000,000 ft^3, allow for heavier payloads at higher altitudes. In support of these larger designs, the importance of accurate aerodynamic data is critical to define design requirements and fully characterize the aerodynamic behavior. With the larger designs that can withstand 100 knot wind environments, the historic wind tunnel database was nearly two orders of magnitude lower in Reynolds number than actual flight conditions. The Reynolds number has a significant effect on drag and therefore an update to the aerodynamic database was needed. This established the requirement for a wind tunnel test at higher speeds and a larger model than had previously been used. Also, the development of an aerostat exceeding 120 meters (m)

[1] Senior Engineering Analyst, Aerostat Systems Department, 7115 Thomas Edison Drive, Non-Member AIAA.
[2] Fellow Engineering Analyst, Aerostat Systems Department, 7115 Thomas Edison Drive, Non-Member AIAA.

in length is currently underway with combinations of shapes that have not been fully wind tunnel tested. The historical aerodynamics and methods for similar, but smaller aerostat and airship shapes are found in Ref. 1 to 6.

The update of the aerodynamic database will continue to build upon and validate historical analysis tools, in particular for the larger aerostats. The TCOM historical analysis tools include:

1) TCOM's static aerostat performance program named FLIGHT
2) TCOM's 6-degree-of-freedom, Non-Linear Dynamic Simulation program named NLDS
3) CFD (pressure distributions for the FEM structural analyses may be obtained from either CFD runs that are validated with wind tunnel data or directly from the wind tunnel pressure distributions).

The test was conducted in the Glenn L. Martin Wind Tunnel at the University of Maryland in College Park, MD from September 20 to October 15, 2010. Wind tunnel tests included variations in angle of attack, angle of sideslip, speeds, and configurations. Configuration variations included a lower anhedral angle of the lower fins for improved mooring clearance. The test goals were met and a valid data set was obtained. The quality of the new data is as good or better when compared to the historical database and the aerostat hull, windscreen, and fin module effects were accurately measured. The data obtained included:

1) force and moment coefficients
2) pressure distributions
3) flow visualizations.

II. Wind Tunnel Test: Setup

The test facility, model, and test plan are detailed in the following three sections.

A. Test Facility

From 1981-2005, wind tunnel tests were performed at the University of Toronto Institute for Aerospace Studies under Dr. DeLaurier. The UT facility had served TCOM well historically, however a larger wind tunnel was needed to expand the Reynolds number range which resulted in choosing the GLM Wind Tunnel for this test. The benefits of the GLM Wind Tunnel include larger size capability, faster speeds, larger angle sweeps, and closer proximity to TCOM. The GLM Wind Tunnel test facility characteristics are as follows:

1) test section is 7.75 ft high by 11.04 ft wide with corner fillets, resulting in a test section area of 85.04 ft^2
2) speed range is 2 mph to 230 mph
3) sphere test turbulence factor is 1.05
4) hot wire measured intensity is 0.21%
5) six component yoke type external balance.

Fig. 1 shows the benefits of reduced Reynolds number scaling with the GLM wind tunnel test. Fig. 1 shows typical operational lines for the conceptual ~120 meter long full scale aerostat at operating altitudes of Sea Level (SL) and 15000 feet (15k). For comparison, Fig. 1 also shows the historical and GLM sub scale data labeled with the length of the each model in meters and the initials of each facility. By comparing the scaling required using only historic sub scale tests and using the GLM 2010 wind tunnel test, the order of magnitude improvement of the GLM test can be seen. Note that the sub scale facilities in Fig. 1 are as follows:

1) NSWC is the Naval Surface Warfare Center Wind Tunnel of the Carderock Division in Maryland
2) Davidson is the Davidson Rotating Arm Water Tank at the Stevens Institute of Technology in New Jersey
3) UT is the University of Toronto Institute for Aerospace Studies Wind Tunnel in Ontario
4) GLM is the Glenn L. Martin Wind Tunnel in Maryland that is the subject of this paper.

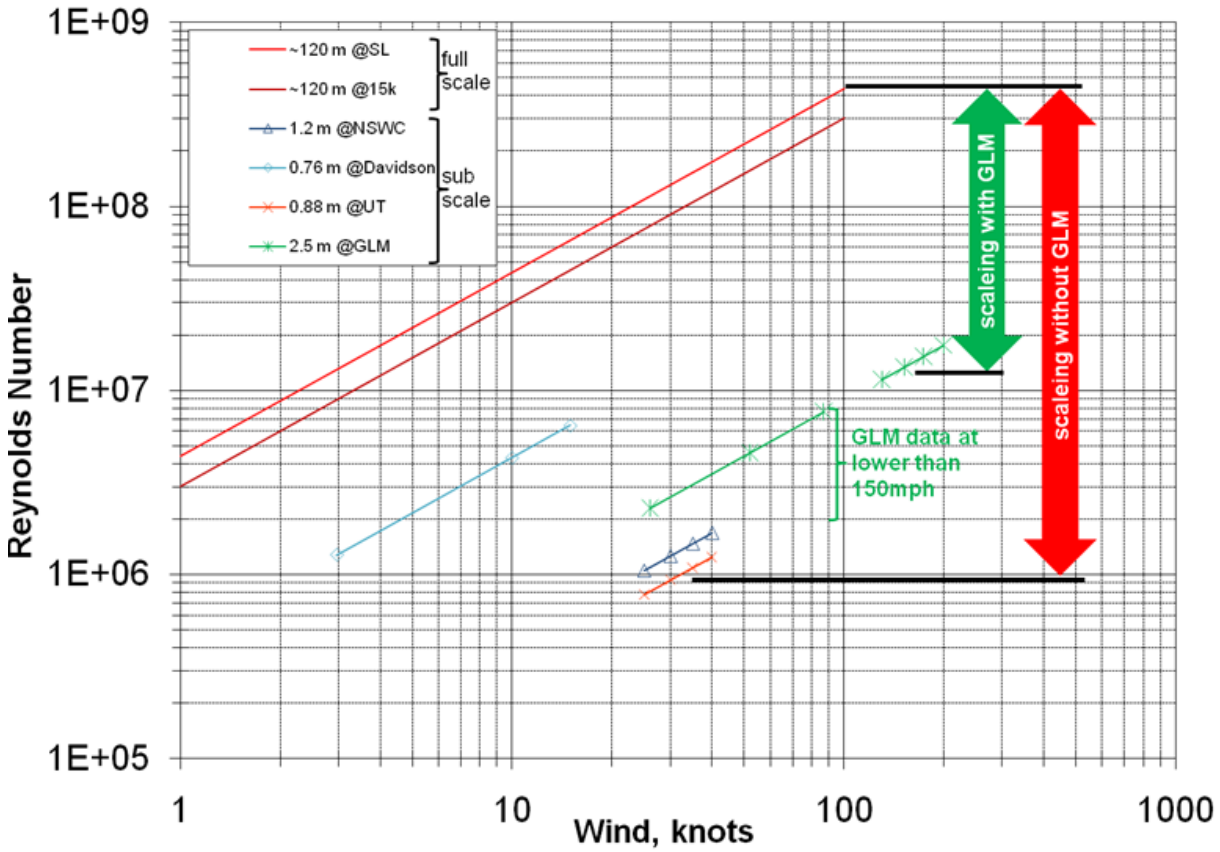

Figure 1. Reynolds number comparison between full scale and sub scale.

B. Model

The wind tunnel model was constructed of a fiberglass shell with internal bulkheads for structural stiffness. The model was attached to the wind tunnel column mount external balance by the model strut. The model strut was a steel rod welded to a plate that was bolted between two of the forward hull bulkheads.

The model is shown in Fig. 2 which was centered in the test section. The 2.5 m chord model was the largest model that could maintain the recommended clearance from the walls of the GLM test section.

The model hull was assembled in 2 main sections:

1) Forward (Fwd) Hull
2) Aft Hull.

Relative to the Fwd Hull, the Aft Hull rotates about the hull axis to set the Phi angle. Therefore, by only rotating the model via the GLM rotatable column mount ($Beta_o$) for various Phi angles, data was obtained for pure Beta sweeps, pure Alpha sweeps and combinations of Beta and Alpha.

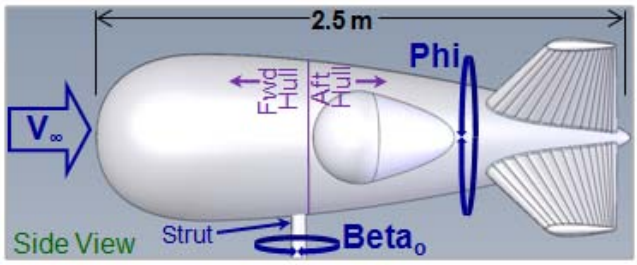

Figure 2. Wind tunnel test model.

The fins and windscreen are detachable allowing for 5 test configurations as shown in Fig. 3a, which consisted of the 3 modules:

1) Hull (H)
2) Windscreen (WS)
3) Three Fins with the baseline number of cells (F), the cells are the fin ridges seen in Fig. 2.

The two fin anhedral angles for the lower fins differentiate configurations 4 and 5 as shown in Fig. 3b. Note that some of the previous literature (such as Ref. 1) has referred to the angle of the lower fins as dihedral. In terms of aircraft, dihedral refers to the angle above the horizontal while anhedral refers to the angle below the horizontal.

Therefore, to be consistent with this aircraft convention, the angle of the lower fins will be referred to as the anhedral angle.

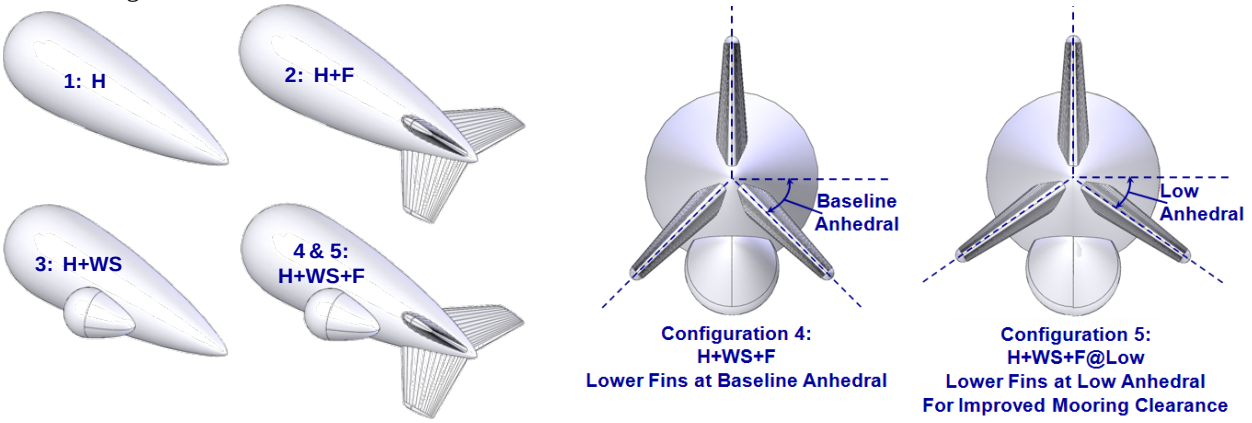

a) Configurations: 1 thru 5. **b) Difference between configurations: 4 & 5.**

Figure 3. Model configurations.

As seen in Fig. 4, 80 pressure taps were primarily placed at the four 90 degree circumferential quadrants to obtain comprehensive pressure distributions. Taps were not located in the forward hull at 180° since that data would always be influenced by being directly in front of the strut.

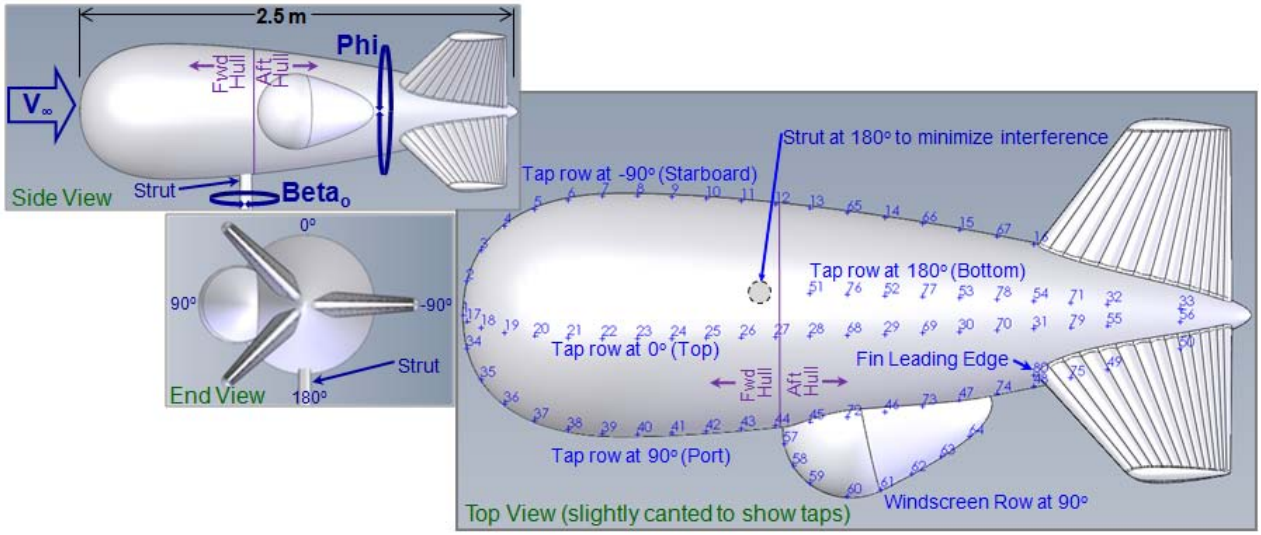

Figure 4. Model pressure tap locations.

C. Test Plan

The wind tunnel test plan consisted of $Beta_o$ sweeps at various Phi angles to obtain for pure Beta sweeps, pure Alpha sweeps, and combinations of Beta and Alpha. Note that the 150 mph speed was chosen for the majority of the test, since that was the maximum speed where the model could have the full $Beta_o$ sweep from -30° to 30° without exceeding the facility force balance limits. Once the speed was greater than 150 mph, the sweeps were lowered to the reduced sweep from -5° to 5° for a few data points to examine the higher speed effects. Several configurations were tested with speeds ranging from 30 to 100 mph to examine slower speed effects.

The two reference parameters for reducing the wind tunnel data are as follows:

1) c = 2.5 m
2) S = 0.77 m^2

Example calculations for the standard aerodynamic coefficients are as follows:

1) C_p = Pressure/(0.5*density*$velocity^2$*S)
2) C_L = Lift/(0.5*density*$velocity^2$*S)

3) C_D = Drag/(0.5*density*velocity^2*S)
4) C_m = Pitching_Moment/(0.5*density*velocity^2*S*c), note that all moments are taken about the nose
5) C_n = Yawing_Moment/(0.5*density*velocity^2*S*c), note that all moments are taken about the nose.

III. Wind Tunnel Test Results

In the following three sections, the wind tunnel test results are detailed which consist of the force and moment data, pressure distribution data, and the flow visualization.

A. Force and Moment Data

The GLM wind tunnel test results compare well with the historic database. Also, the GLM wind tunnel test results show that the effects of each parameter were properly measured. The parameters include speed variation and configurations (including measurements for the effects of fin anhedral angle and the effects of each separate module).

Fig. 5 to Fig. 14 show the force and moment coefficients vs. the 2 main angle sweeps of Alpha and Yaw in degrees. Therefore, the effect of each parameter should be seen by examining the set of Alpha and Yaw sweeps which is the reason that Fig. 5 to Fig. 14 are each numbered as an a) and b) set:

a) Alpha (α):
    1. C_D = drag force coefficient
    2. C_L = lift force coefficient
    3. C_m = pitching moment coefficient
b) Yaw (ψ):
    1. C_D = drag force coefficient
    2. C_S = side force coefficient
    3. C_n = yawing moment coefficient

Note that Yaw was chosen instead of Beta for ease of examining the 2 figures as a set since plotting vs. Yaw would result in the trends being plotted in the same direction for:

1) C_L and C_S
2) C_m and C_n.

Also note that all of the data is from the 2010 GLM wind tunnel test at the baseline speed of 150 mph and for the baseline configuration (H+WS+F) with the lower fins at baseline anhedral angle, unless otherwise noted throughout section III.A. The force and moment coefficient plots also have consistent color coding throughout section III.A.

1. Comparison to Historical Database

Fig. 5 and 6 show the comparison of the GLM 2010 (solid lines) and University of Toronto Institute for Aerospace Studies (dotted lines) historical tests from 1998 and 2005. As seen in these figures, the trends of the data are similar for all tests. The small differences can be attributed to the testing of differently shaped models and minor facility differences. For example in Fig. 6b, the higher UT 2005 C_D is caused by testing fewer-celled fins vs. the GLM fins. The fewer-celled fins have been shown in other TCOM wind tunnel tests to have higher drag due to the lower number of larger cells which result in more disturbed flow over the fins. The aerodynamic effects of fewer-celled fins were examined and trade studies balanced performance, manufacturing, and structural considerations which resulted in fewer-celled fins to be used on various aerostats. In addition, the drag values from this test also compare well with the drag values found in the Ref. 1 to 6.

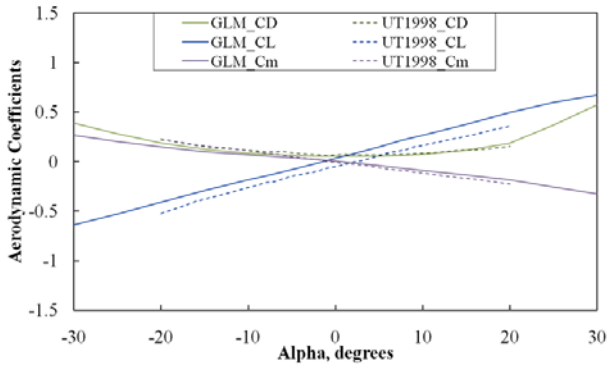

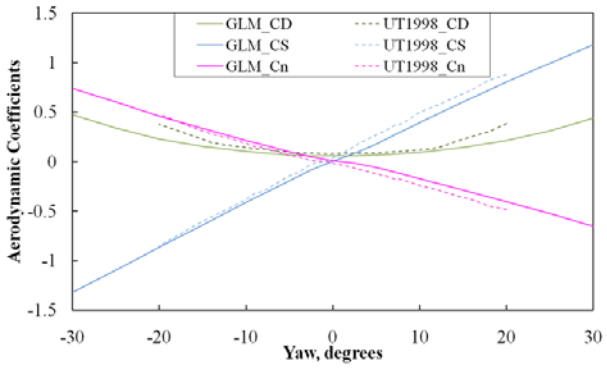

a) Alpha Sweep **b) Yaw Sweep**

Figure 5. Comparison to University of Toronto 1998.

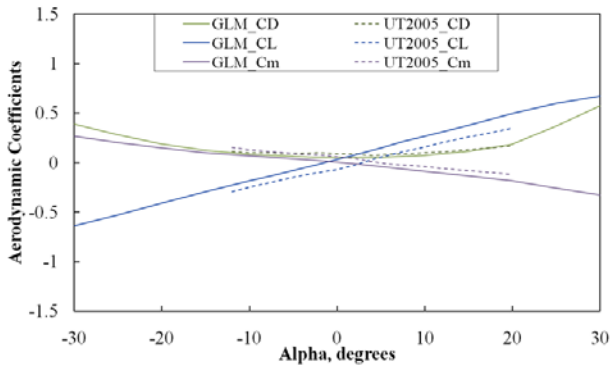

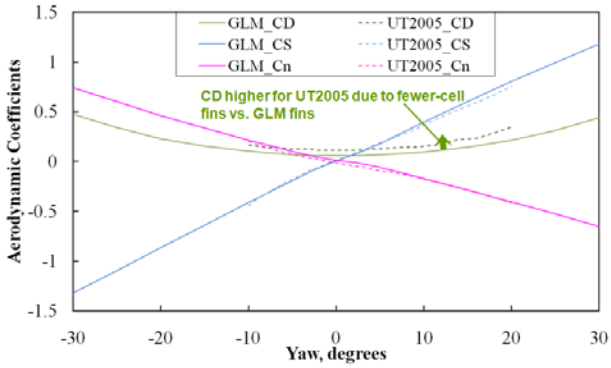

a) Alpha Sweep **b) Yaw Sweep**

Figure 6. Comparison to University of Toronto 2005.

2. Speed Effects

Fig. 7 shows the speed effects for greater than the baseline of 150 mph, which are small for the lower angle sweep range of -5° to 5°. Fig. 8 shows the speed effects for less than the baseline of 150 mph, which are more significant for the full angle sweep range of -30° to 30°. For instance, the drag increase for the higher skin friction drag at the lower speeds is seen. The Reynolds number drag scaling accounts for the predominant effect of decreased skin friction at the higher Reynolds numbers as described in Ref. 7, which is relevant for turbulent flows that are typical in the aerostat operating environment. Therefore, this historical Reynolds number drag scaling to the full scale environment is validated and will continue to be used. As seen in Fig. 1, the GLM increase in speed and size brings the TCOM aerodynamic database to approximately an order of magnitude of the full scale Reynolds number which leads to far less Reynolds number drag scaling than previously required.

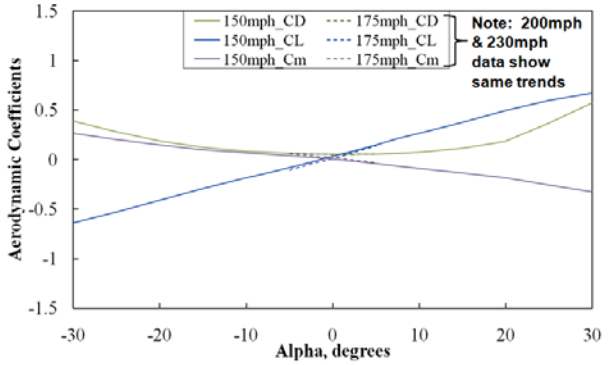

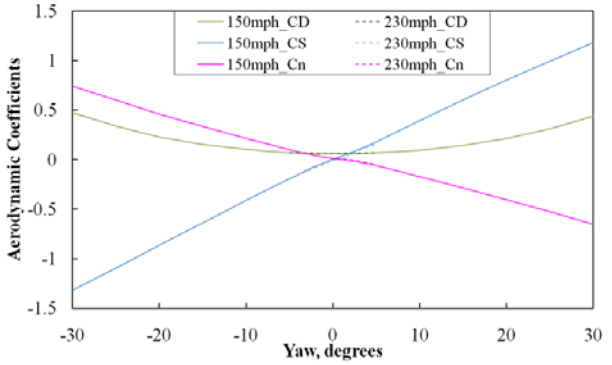

a) Alpha Sweep **b) Yaw Sweep**

Figure 7. Speed effects for more than the baseline of 150 mph.

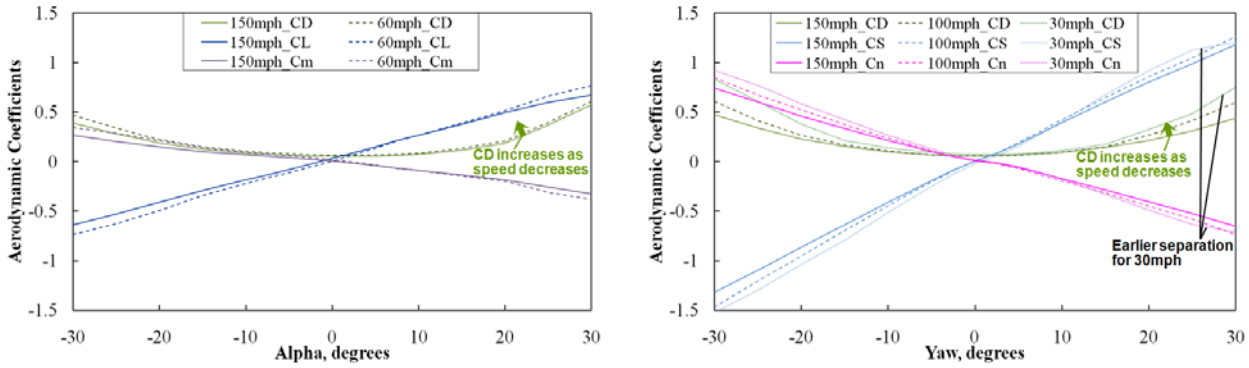

a) Alpha Sweep **b) Yaw Sweep**

Figure 8. Speed effects for less than the baseline of 150 mph.

3. Fin Anhedral Angle Effects

Fig. 9 shows the fin anhedral angle effects. The effects are as expected in that the lower anhedral angle fins act more like horizontal tails in Fig. 9a and act less like vertical tails in Fig. 9b. Since these effects are as expected, once these fin anhedral angle effects are analyzed by running the FLIGHT and NLDS analysis programs with the updated aerodynamic database, trade studies can be made between the fin anhedral angles.

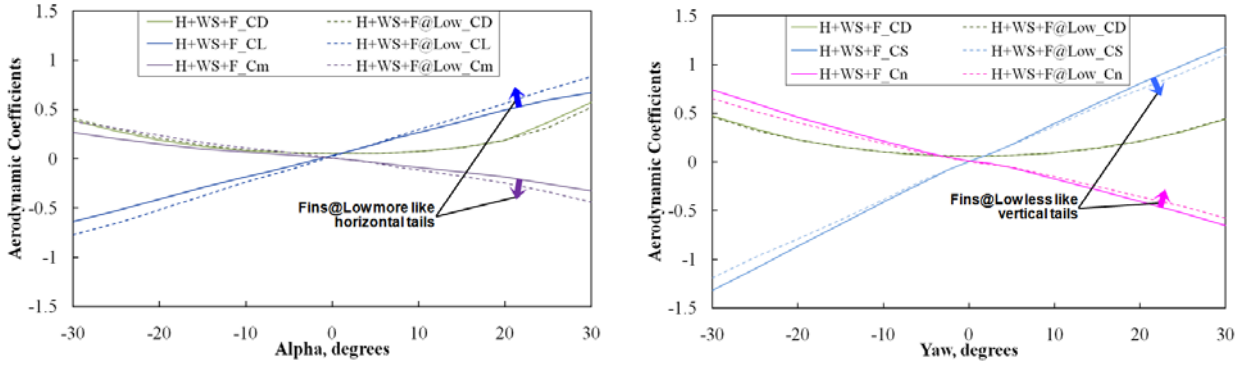

a) Alpha Sweep **b) Yaw Sweep**

Figure 9. Fin Anhedral Angle Effects.

4. Hull, Windscreen and Fin Module Effects

As will be detailed below, the hull, windscreen and fin module effects were accurately measured. For example, the C_D can be seen to increase when modules are added to the H (+WS, +F or +WS+F) throughout section III.A.4. Additional examples of accurate measurements are discussed for each configuration below.

a. Fin Module Effects

Fig. 10 shows the fin effects. Fig. 10a effects are as expected in that with no fins, all the coefficients decrease and the decrease is fairly large for the longitudinal coefficients (C_m and C_L). Fig. 10b effects are as expected in that with no fins, all the coefficients decrease and the decrease is largest for the lateral coefficients (C_n and C_S) as compared to Fig. 10a, since the fins effects are dominant for the lateral coefficients. Both Fig. 10a and Fig. 10b underscore the importance of accurate fin modeling for overall aerostat stability.

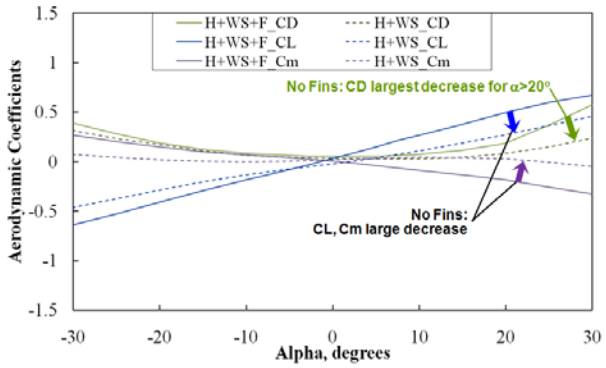

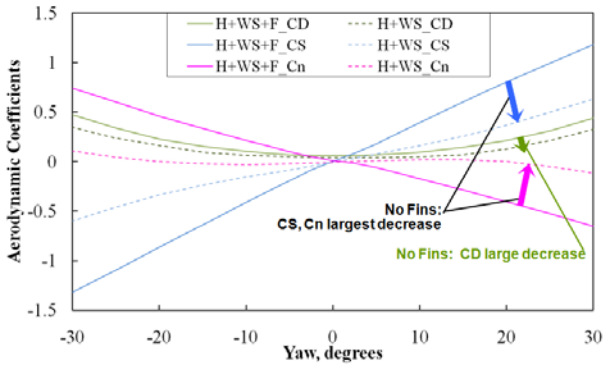

a) Alpha Sweep **b) Yaw Sweep**

Figure 10. Fin effects.

Fig. 11 compares the H+F vs. H to remove the effect of the windscreen. Fig. 11 is nearly identical to Fig. 10 which shows the small effect of the windscreen, especially for the Alpha sweep. Fig. 11 also shows that the bare hull is typically only stable at low angles and therefore the importance of the fins in overall aerostat stability is again underscored.

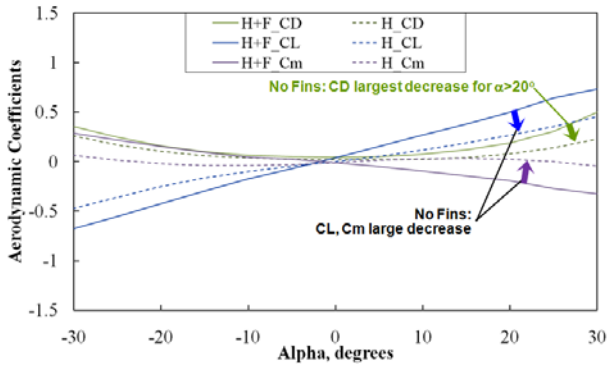

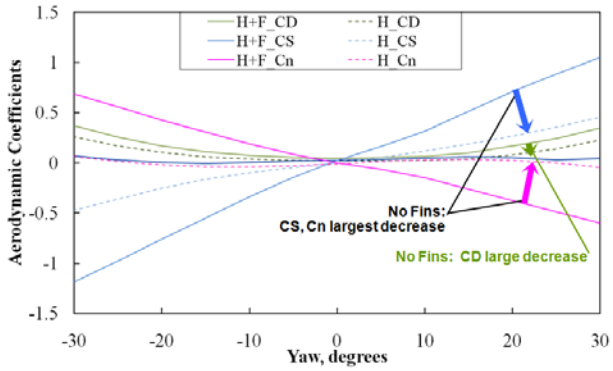

a) Alpha Sweep **b) Yaw Sweep**

Figure 11. Fin effects on bare hull.

b. Windscreen Effects

Fig. 12 shows the windscreen effects. The drag results are as expected in that C_D decreases slightly with no windscreen in both Fig. 12a and Fig. 12b. In Fig. 12b, the results are again as expected since both C_S and C_n decrease with no windscreen which shows that the windscreen improves lateral stability since it acts like a dorsal fin. Historical comparison of windscreen effects on C_D is also favorable as compared to Ref. 1 and 4. Note that in comparing Fig. 10 and Fig. 12, it is seen that the windscreen has a much smaller effect than the fins in both the Alpha and Yaw Sweeps, as expected.

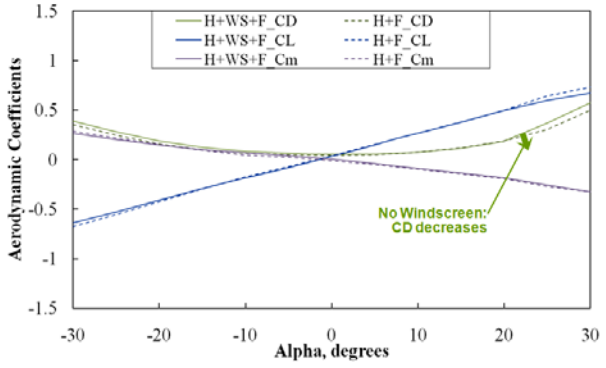

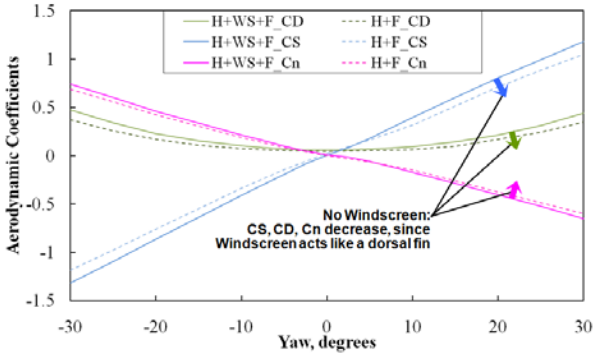

a) Alpha Sweep **b) Yaw Sweep**

Figure 12. Windscreen effects.

In order to remove the fins trends from the plots, Fig. 13 shows the windscreen effects by comparing the H+WS vs. H only. The results are as expected in that that C_D decreases with no windscreen in Fig. 13. The other coefficients are more difficult to compare since the H+WS and H configurations do not have the stabilizing effect of the fins.

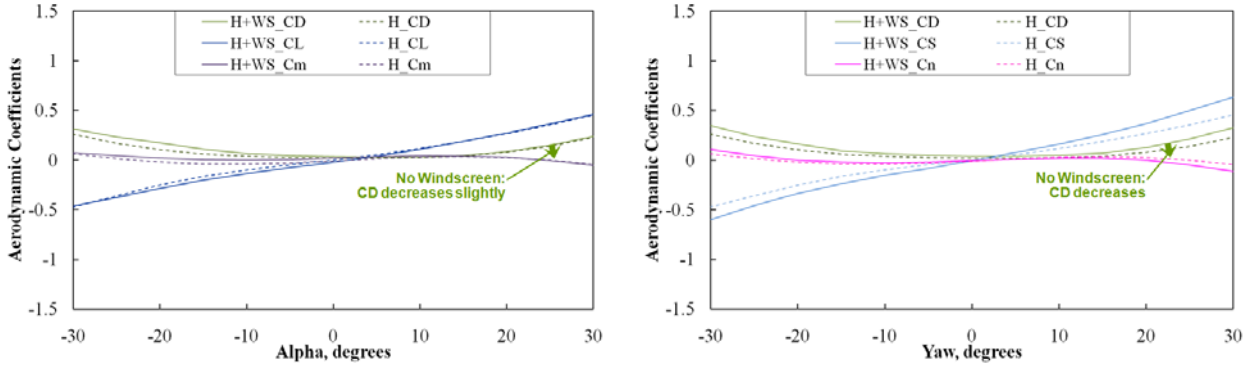

a) Alpha Sweep **b) Yaw Sweep**

Figure 13. Windscreen effects on bare hull.

c. Combined Windscreen and Fin Effects

Fig. 14 shows the combined fin and windscreen effects. The contributions of fins to the improved aerostat longitudinal coefficients (C_m and C_L) are seen in Fig. 14a when compared to the bare hull. Fig. 14b effects are as expected in that with no fin and no windscreen, all the coefficients decrease and the decrease is largest in Yaw (C_S and C_n) as compared to Fig. 14a, since the fins and windscreen effects are dominant for the lateral coefficients. These trends are similar to those seen in Fig. 10, Fig. 11, Fig. 12, and Fig. 13.

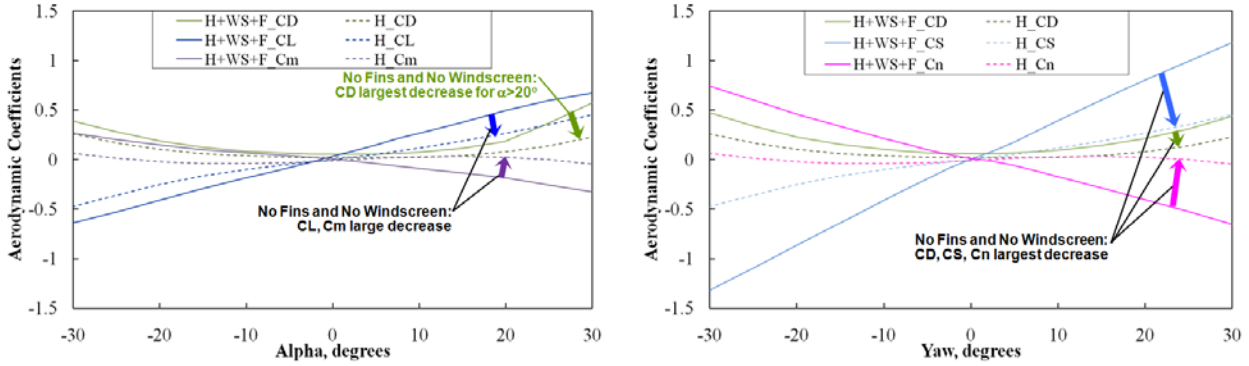

a) Alpha Sweep **b) Yaw Sweep**

Figure 14. Combined fin and windscreen effects on bare hull.

B. Pressure Distribution Data

Sample pressure distribution plots for the H only configuration are seen in Fig. 15 and Fig. 16. Fig. 15 shows the expected symmetric distribution since the bare hull is at Yaw=0^o and Alpha=0^o. Just aft of the strut, the localized strut effects are seen in that the four pressures distributions do not lie perfectly on top of one another. Fig. 16 is an example pressure distribution for the H only configuration at Yaw=30^o and Alpha=0^o where the large negative and positive pressure regions are seen in the leeward and windward sides of the front of the hull, respectively (similar to an airfoil or other streamline body.)

Fig. 17 is an example pressure distribution for the H+WS+F configuration at Yaw=0^o and Alpha=0^o, where it can be seen that the distribution is symmetric except near the windscreen and just forward of the fins. The distribution over the windscreen is as expected as shown by the stagnation pressure near tap 57 which is at the leading edge of the windscreen and the large negative pressure centered at tap 60 which is at the largest curvature of the windscreen. Similar windscreen, fin and strut effects are seen in Fig. 16, 17, and Fig. 18 and throughout all of the distributions whenever a component was part of the test configuration.

Fig. 18 is an example pressure distribution for the H+WS+F configuration at Yaw=30^o and Alpha=0^o. This distribution is as expected in that it is composed of two main parts. The first part is the large negative and positive pressure regions are seen in the leeward and windward sides of the front of the hull, respectively (similar to Fig. 16). The second part is the similar windscreen distribution as described above for Fig. 17.

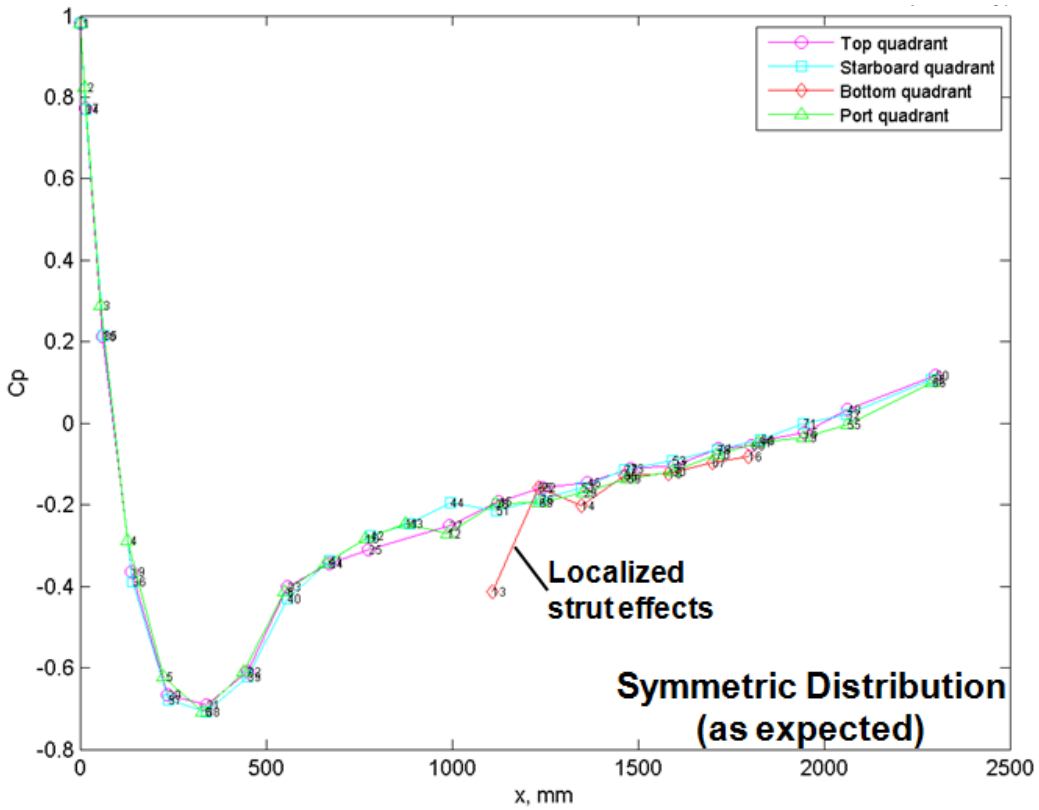

Figure 15. Pressure distribution for the bare hull at Yaw=0° and Alpha=0°

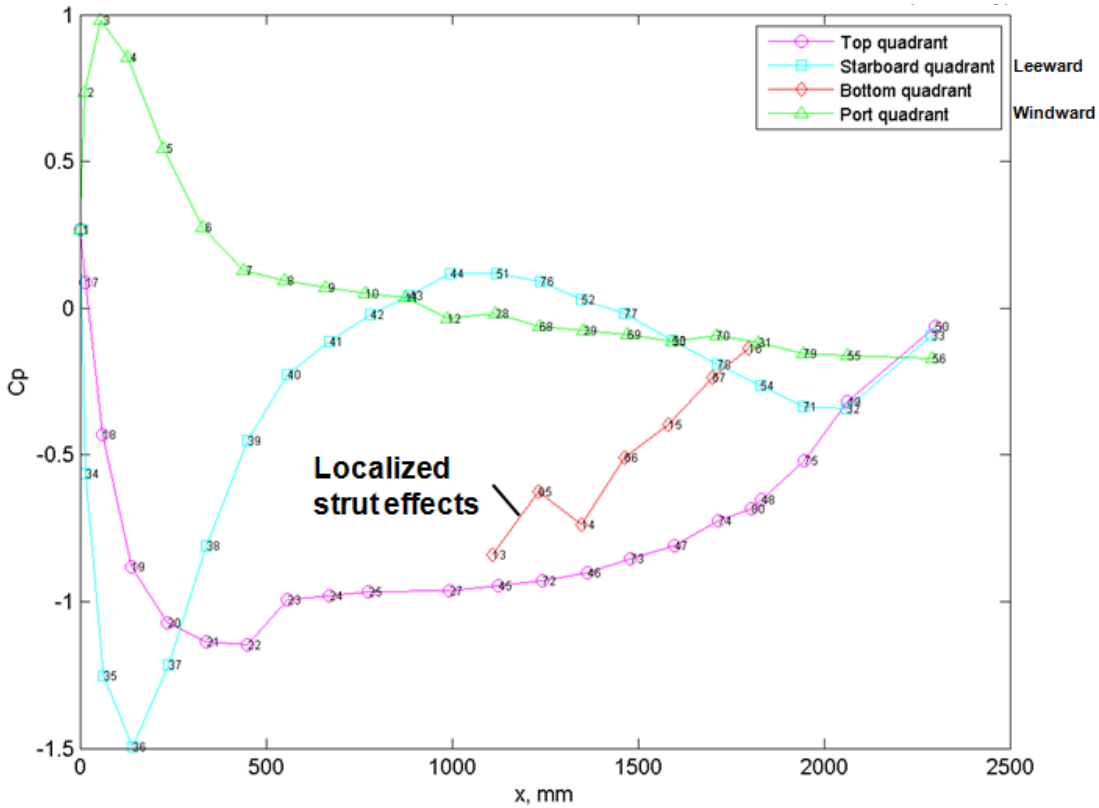

Figure 16. Pressure distribution for the bare hull at Yaw=30° and Alpha=0°

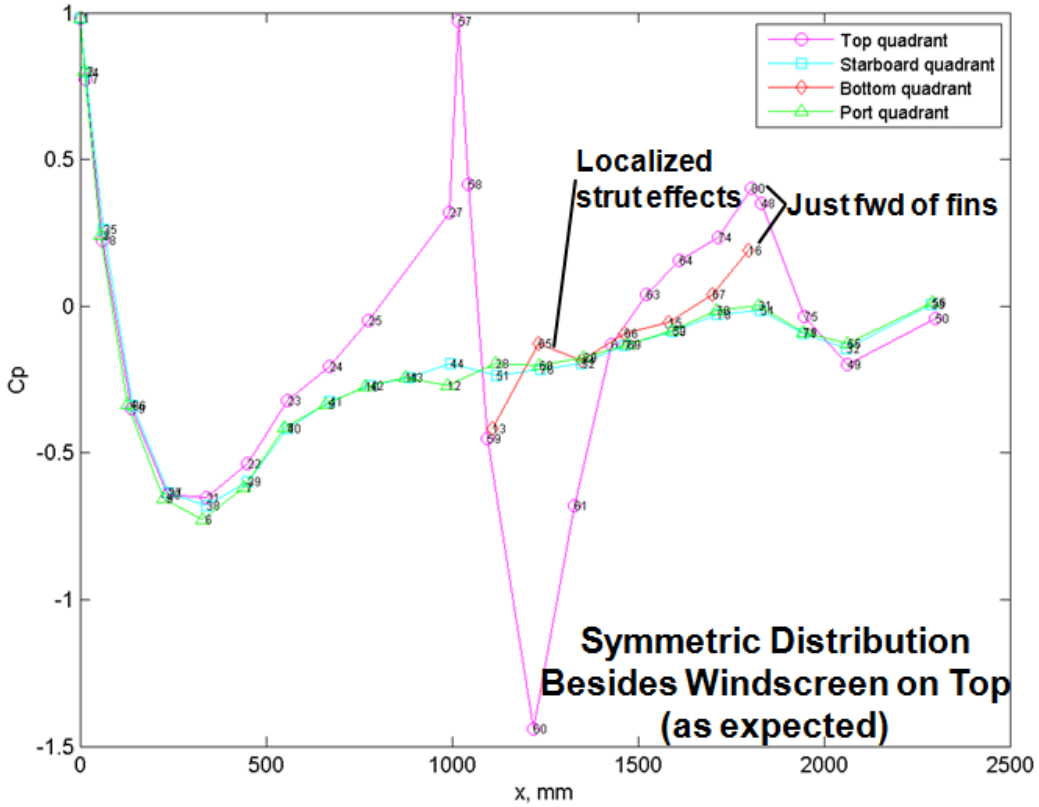

Figure 17. Pressure distribution for the hull, windscreen and fins at Yaw=0^o and Alpha=0^o

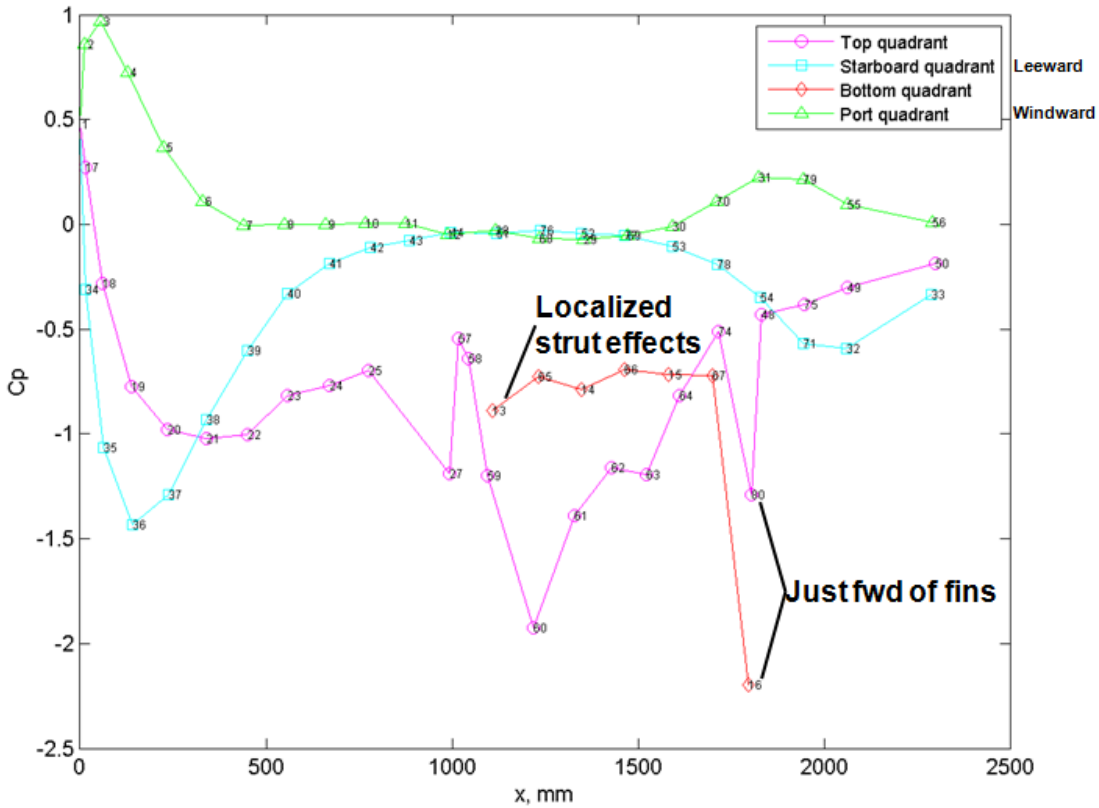

Figure 18. Pressure distribution for the hull, windscreen and fins at Yaw=30^o and Alpha=0^o

C. Flow Visualizations

Flow visualization movie files (*.AVI) with a single stream smoke wand were taken with a digital camera. A snapshot of the flow visualization is shown in Fig. 19. The flow visualization provides qualitative verification of the aerodynamics. For example, it can be seen that the strut effects are fairly localized so that GLM historical method of subtracting the tares and interference strut deltas is valid. Also, the flow visualizations confirmed that the flow over the aerostat is well behaved. In fact, the flow visualization movie files show that even at Yaw=30^o and Alpha=0^o, the flow over the leeward fin remains largely attached.

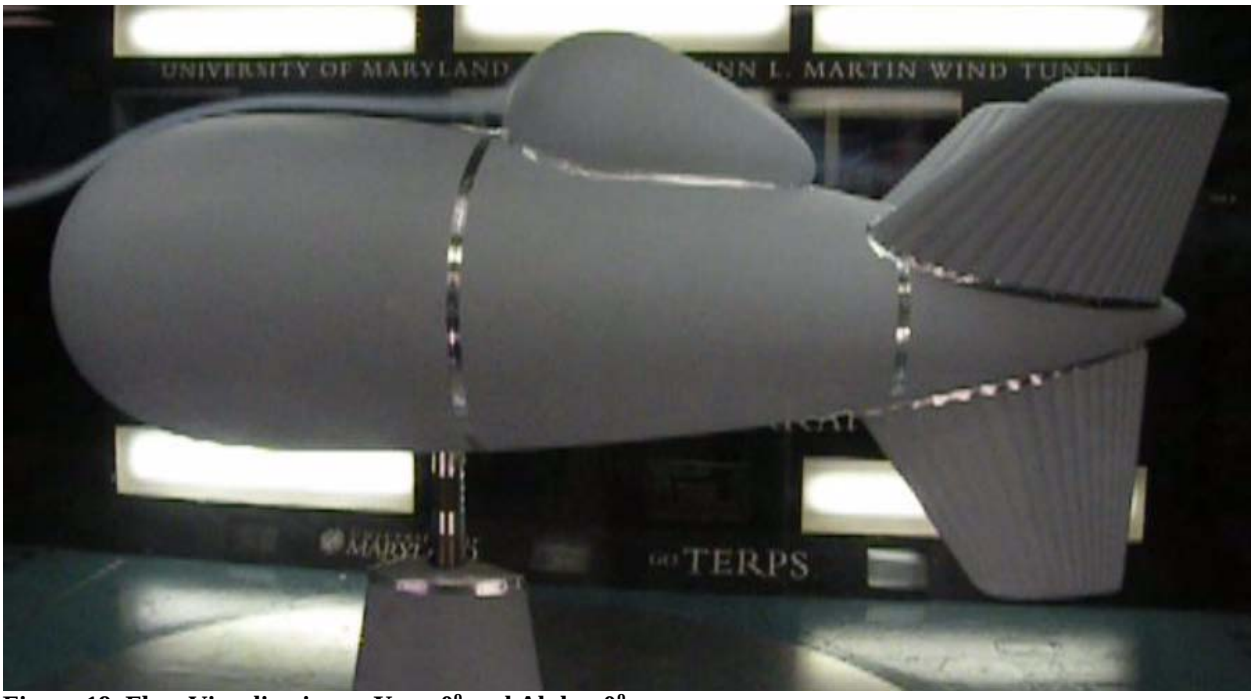

Figure 19. Flow Visualization at Yaw=0^o and Alpha=0^o

D. Data Reduction

The reduction of the wind tunnel data for incorporation into the simulation programs FLIGHT and NLDS was done in accordance with the methods in Ref. 1, 8, and 9. These methods included Reynolds number drag scaling which accounts for the predominant effect of decreased skin friction at the higher Reynolds numbers as described in Ref. 7. The results of this wind tunnel test compare favorably to Ref. 4. Also, an independent review was conducted by Dr. DeLaurier in December 2010 who concluded that the test and the results were valid.

IV. Conclusion

The 2010 GLM force and moment data, pressure distributions, and the flow visualization is a valid set to use in updating the aerodynamic database. The trends are as expected and the Reynolds number drag scaling is improved by an order of magnitude over historical tests. Also, the pressure distributions show the proper trends and are appropriate to use to validate the CFD and as inputs to FEM structural analyses on aerostat systems.

References

[1] Jones, S.P., "Aerodynamics of a New Aerostat Design with Inverted-Y Fins", AIAA Paper 85-0867-CP, AIAA 6th Lighter-Than-Air Systems Conference, Norfolk, VA, 26-28 Jun. 1985.

[2] Badesha, S., and Jones, S.P., "Aerodynamics of the TCOM 71M Aerostat", AIAA Paper 93-4036-CP, 10th AIAA Lighter-Than-Air Systems Technology Conference, Scottsdale, AZ, 14-16 Sep. 1993.

[3] "Aerodynamic Model Tests with German and Foreign Airship Designs in The Wind Tunnel of The Zeppelin Airship Works at Friedrichshafen," ZWB Report FB. No. 1647 (Translated), Apr. 1942.

[4] Hoerner, S., *Fluid-Dynamic Drag*, Published by the Author, 1958, pp.3-8, 6-6, 6-17.

[5] Kale, S. M., and Joshi, P., "A Generic Methodology For Determination Of Drag Coefficient Of An Aerostat Envelope Using CFD", 5th AIAA\ATIO and 16th Lighter-Than-Air Systems Technology Conference and Balloon Systems Conference, Crystal City, Arlington, Sep. 2005.

[6] Buerge, B. T., “The Suitability of Hybrid vs. Conventional Airships for Persistent Surveillance Missions”, AIAA Paper 2010-1014, 48th AIAA Aerospace Sciences Meeting Including the New Horizons Forum and Aerospace Exposition, Orlando, FL, 4-7 Jan. 2010.

[7] Schlichting, H. and Truckenbrodt, E., *Aerodynamics of the Aeroplane*, McGraw-Hill, 1979, pp.91.

[8] Jones, S. P., and DeLaurier. J. D., "Aerodynamic Estimation Techniques for Aerostats and Airships," AIAA Journal of Aircraft, Vol. 20, No. 2, Feb. 1983, pp. 120-126.

[9] Jones, S. P., and DeLaurier J. D., "Lighter-Than-Air Vehicles," Chapter: Fluid-Dynamic Related Technologies, Handbook of Fluid Dynamics and Fluid Machinery, Vol. 3, Applications of Fluid Dynamics, Edited by Joseph A. Schetz and Allen E. Fuhs, John Wiley and Sons, 1996 pp. 1741-1755.